Intercomparison of Soil Moisture Memory in Two Land Surface Models

SARITH P. P. MAHANAMA

Goddard Earth Sciences and Technology Center, University of Maryland, Baltimore, Baltimore, and Hydrological Sciences Branch, NASA Goddard Space Flight Center, Greenbelt, Maryland

RANDAL D. KOSTER

Hydrological Sciences Branch, NASA Goddard Space Flight Center, Greenbelt, Maryland

(Manuscript received 5 February 2003, in final form 22 April 2003)

ABSTRACT

A heavy rain or a dry period can produce an anomaly in soil moisture, and the dissipation of this anomaly may take weeks to months. It is important to understand how land surface models (LSMs) used with atmospheric general circulation models simulate this soil moisture ''memory,'' because this memory may have profound implications for long-term weather prediction through land–atmosphere feedback.

In order to understand better the effect of precipitation and net radiation on soil moisture memory, the NASA Seasonal-to-Interannual Prediction Project (NSIPP) Catchment LSM and the Mosaic LSM were both forced with a wide variety of idealized climates. The imposed climates had average monthly precipitation ranging from 15 to 500 mm and monthly net radiations (in terms of water equivalent) ranging from 20 to 400 mm, with consequent changes in near-surface temperature and humidity. For an equivalent water holding capacity, the two models maximize memory in distinctly different climate regimes. Memory in the NSIPP Catchment LSM exceeds that in the Mosaic LSM when precipitation and net radiation are of the same order; otherwise, memory in the Mosaic LSM is larger.

The NSIPP Catchment and the Mosaic LSMs were also driven offline, globally, for a period of 15 yr (1979–93) with realistic atmospheric forcing. Global distributions of 1-month-lagged autocorrelation of soil moisture for boreal summer were computed. An additional global run with the NSIPP Catchment LSM employing the Mosaic LSM's water holding capacities was also performed. These three global runs show that while some of the intermodel difference in memory can be explained (following traditional interpretations) in terms of differences in water holding capacity and potential evaporation, much of the intermodal difference stems from differences in the parameterizations of evaporation and runoff.

1. Introduction

A period of heavy rainfall or drought can produce an anomaly in soil moisture that may take weeks or months to dissipate. In effect, the soil can ''remember'' the wet or dry weather conditions that caused the anomaly long after these conditions are forgotten by the atmosphere. Soil moisture memory can be characterized in various ways, including anomaly decay timescales and 1-month-lagged moisture autocorrelations.

Long-term records of soil moisture are not available in many parts of the world, and thus our ability to quantify soil moisture memory from soil moisture observations is strongly limited. The Global Soil Moisture Data Bank (Robock et al. 2000), however, does have substantial data, mainly in Asia. Soil moisture anomaly decay timescales of 2–3 months have been derived by analyzing in situ soil moisture data from stations in Russia (Vinnikov and Yeserkepova 1991; Vinnikov et al. 1996). Entin et al. (2000) derived timescales of about 2 months from Chinese, Mongolian, and Illinois data. Available data show that the timescales of soil moisture anomaly dissipation vary spatially (Vinnikov and Yeserkepova 1991), presumably due to spatial variability of surface characteristics and prevailing climatic conditions.

Soil moisture memory is particularly relevant to the seasonal prediction of precipitation, temperature, and other meteorological variables. This is because the persistence of a soil moisture anomaly into a forecast period allows the anomaly to influence meteorological variables during the forecast period—various modeling studies (e.g., Shukla and Mintz 1982; Oglesby and Erickson 1989; Koster and Suarez 1995, 1996b; Liu and Avissar 1999a,b; Dirmeyer 2000) have shown that the atmosphere responds somewhat predictably to anomalies in land surface moisture state. Indeed, initializing the land surface in a seasonal forecasting system may

Corresponding author address: Sarith Mahanama, Global Modeling and Assimilation Office, NASA Goddard Space Flight Center, Code 900.3, Greenbelt, MD 20771.
E-mail: sarith@janus.gsfc.nasa.gov

be as useful as initializing the system's coupled ocean model, particularly for summer forecasts in transition zones between dry and humid regions (Koster et al. 2000b).

The land surface model (LSM) of a seasonal forecasting system performs the water and energy budget calculations over the land surface and is thereby responsible for determining (and taking advantage of) soil moisture memory. Simulated memory can, in fact, be strongly LSM-dependent, and this can lead to forecast error. Depending on its structure, an LSM may underestimate memory relative to nature, thereby underestimating predictability in the system, or it may overestimate memory, leading to overconfident seasonal predictions. When relying on land moisture initialization in a seasonal prediction system, the nature of the LSM's simulated soil moisture memory must be well understood.

Delworth and Manabe (1988) pioneered the study of soil moisture memory in AGCMs, using a first-order Markov process model to relate memory to potential evaporation and soil water holding capacity. Koster and Suarez (2001) provide a more comprehensive equation that relates soil moisture autocorrelation to four separate features of the physical system: 1) seasonality in the statistics of the atmospheric forcing, 2) the sensitivity of evaporation to soil moisture in the LSM, 3) the sensitivity of runoff to soil moisture in the LSM, and 4) correlation of forcing with antecedent soil moisture. (See section 2.) They successfully tested the equation on the global scale against atmospheric general circulation model (AGCM) data. The equation provides a quantitative framework for analyzing a given LSM's memory characteristics and for pointing out how deficiencies in the LSM–atmosphere system may compromise the simulation of memory.

A potential, yet untested, value of the equation lies in its use to contrast the memory characteristics of different LSMs. Why, under the same atmospheric forcing, does one LSM preserve a soil moisture anomaly longer than another? Can we evaluate which LSM has the more realistic memory based on the factors that control it? In the present paper, through a series of ''offline'' experiments, we use the equation to contrast the memory behavior of the Mosaic LSM (Koster and Suarez 1996a) and the fundamentally different National Aeronautics and Space Administration (NASA) Seasonal-to-Interannual Prediction Project (NSIPP) Catchment LSM (Koster et al. 2000a). In the first experiment (section 3), a wide range of idealized precipitation and radiation forcing is applied to each LSM. The two LSMs are found to respond quite differently to the forcing; certain climatic regimes favor memory in the Mosaic LSM, whereas other regimes favor memory in the NSIPP Catchment LSM. The autocorrelation equation allows us to explain this climate dependence. In the second experiment (section 4), global arrays of realistic atmospheric forcing are applied to each model. This results not only in global arrays of soil moisture memory for each model, which can be directly compared, but also in global arrays of the factors that control each model's memory. Given the dearth of soil moisture observations on the global scale, it is the evaluation of these factors that may someday lead to an evaluation of the accuracy of simulated soil moisture memory.

2. Soil moisture autocorrelation equation

Here, we explain the basis of the soil moisture autocorrelation equation used later in this study. The reader is referred to Koster and Suarez (2001) for a more detailed description of its derivation. Koster and Suarez (2001) assumed that the water balance for the soil column of a typical LSM, for time period of n of year y, can be written (in the absence of snow) as

$$C_s w_{n+1,y} = C_s w_{n,y} + P_{n,y} - E_{n,y} - Q_{n,y}, \qquad (1)$$

where C_s is the column's water holding capacity, w_n is the average degree of saturation in the column as a whole (instantaneous value at the beginning of time period n), P is precipitation, E is the total evaporation (which includes transpiration, bare soil evaporation, and interception loss), and Q is the total runoff (which includes both surface and subsurface runoff). The values P, E, and Q are accumulated fluxes during time period n. The evaporation and runoff fluxes generated by any LSM typically reflect complex parameterizations involving numerous state variables and parameters. Nevertheless, following the approach of Koster and Milly (1997), we approximate the dependence of evaporation and runoff on soil moisture with simple empirically fitted linear functions:

$$\frac{Q_{n,y}}{P_{n,y}} = a\left(\frac{w_{n,y} + w_{n+1,y}}{2}\right) + b, \quad \text{and} \qquad (2)$$

$$\frac{E_{n,y}}{R_{n,y}} = c\left(\frac{w_{n,y} + w_{n+1,y}}{2}\right) + d. \qquad (3)$$

Here, R is the accumulated net radiation during the month n (normalized by the latent heat of vaporization, to have the same units as E). The empirically derived, LSM specific parameters a, b, c, and d are established through analysis of several years of model simulations.

Equations (2) and (3) are substituted into (1). Then, by separating w, P, and R into their mean components for the given time of year (indicated by over lines) and corresponding interannual anomalies, the result simplifies to the following semi-implicit equation:

$$\rho = \frac{\mathrm{cov}(w_n, w_{n+1})}{\sigma_{w_n}\sigma_{w_{n+1}}} = \frac{\sigma_{w_n}}{\sigma_{w_{n+1}}}\left[\frac{2 - \frac{c\overline{R_n}}{C_s} - \frac{a\overline{P_n}}{C_s}}{2 + \frac{c\overline{R_n}}{C_s} + \frac{a\overline{P_n}}{C_s}} + \frac{\mathrm{cov}(w_n, F_n)}{\sigma_{w_n}^2}\right], \qquad (4)$$

where F_n is a particular combination of forcing terms and model parameters. In (4), the autocorrelation of soil moisture is expressed as a function of four distinct terms: (a) $\sigma_{w_n}/\sigma_{w_{n+1}}$, which relates to seasonality in the statistics of the atmospheric forcing; (b) $c\overline{R_n}/C_s$, which relates to the sensitivity of evaporation to soil moisture variations; (c) $a\overline{P_n}/C_s$, which relates to the sensitivity of runoff to soil moisture variations; and (d) $\text{cov}(w_n, F_n)/\sigma^2_{w_n}$, which reflects both the memory of external forcing and land–atmosphere feedback. Therefore, (4) not only helps us estimate ρ, but it also provides a unique means of characterizing the contributions of atmospheric forcing (through $\overline{R_n}$ and $\overline{P_n}$) and the overall structure of the land surface model (through the parameters a, c, and C_s) to soil moisture memory. Koster and Suarez (2001) demonstrate that (4) indeed reproduces the soil moisture autocorrelations generated by the NSIPP AGCM.

3. Models

a. The Mosaic LSM

The Mosaic LSM (Koster and Suarez 1992, 1996a), a derivative of the Simple Biosphere (SiB) Model of Sellers et al. (1986), computes areally averaged energy and water fluxes from the land surface in response to meteorological forcing. The model allows explicit vegetation control over the computed surface energy and water balances, with environmental stresses acting to increase canopy resistance and thus decrease transpiration. The vertical structure of the model includes a canopy interception reservoir and three soil reservoirs: a thin surface layer, a middle layer that encompasses the remainder of the root zone, and a lower ''recharge'' layer at the bottom. Bare soil evaporation, transpiration, and interception loss occur in parallel, and runoff occurs both as overland flow during precipitation events and as groundwater flow out of the recharge layer. A complete snow budget is included. Many components of the model mimic the corresponding components of SiB, in particular the parameterization of stomatal resistance.

The Mosaic LSM accounts for subgrid heterogeneity in surface characteristics by dividing each grid cell into several different subregions, ''tiles,'' each containing a single vegetation or bare soil type. The number and relative sizes of the tiles in a given grid cell are determined from observed vegetation maps. Energy and water balance calculations are performed separately over each relatively homogeneous tile, and each tile maintains its own prognostic variables.

b. The NSIPP Catchment LSM

Most LSMs coupled to atmospheric GCMs effectively consider soil moisture to be spatially uniform over a grid cell, which may span hundreds of kilometers. Runoff generation and subsurface soil moisture movement in nature, however, are largely controlled by the topography of the land surface and small-scale spatial heterogeneity in soil moisture. Even the Mosaic LSM, which breaks a grid cell into subgrid tiles, cannot resolve the relevant soil moisture heterogeneity. Typical surface vegetation–atmosphere transfer (SVAT) models are thus arguably ill-equipped to model runoff correctly [and, by extension, evaporation correctly (Koster and Milly 1997)]. Note also that imposing quasi-rectangular atmospheric grid elements on the land surface itself is a rather artificial representation, because in nature soil moisture movement and runoff generation take place over irregularly shaped, topographically defined hydrologic catchments.

This is the motivation behind the development of a new LSM, the NSIPP Catchment LSM (Koster et al. 2000a; Ducharne et al. 2000). This LSM considers the irregularly shaped hydrologic catchment as the fundamental element on the land surface for computing land surface processes. Each catchment is partitioned into three regimes: 1) a saturated region, from which evaporation occurs with no water stress and over which rainfall is immediately converted to surface runoff, 2) a subsaturated region, from which transpiration occurs with no water stress and over which rainwater infiltrates the soil, and 3) a ''wilting'' region, in which transpiration is shut off. The relative areas of these regions vary dynamically; they are unique functions of the NSIPP Catchment LSM's three water prognostic variables and the topographic characteristics of the catchment. By continually partitioning the catchment into hydrologically distinct regimes and then applying different regime-appropriate physics within each regime, the Catchment LSM should, at least in principle, provide a more realistic representation of surface energy and water processes.

4. Experiments

a. Idealized experiment: Sensitivity of soil moisture memory to climatic conditions

The impact of different climate conditions on the autocorrelation of soil moisture is investigated here in an idealized, perpetual-July experiment. By the construct of the experiment, two of the four controls identified in (4), namely, those associated with seasonality and persistence in the statistics of the atmospheric forcing, have little impact on the simulated autocorrelation of soil moisture. This experiment is instead designed to investigate the impact of the evaporation and runoff terms on soil moisture autocorrelation under a wide variety of monthly precipitation and net radiation rates. For simplicity, all soil properties (including water holding capacity) and vegetation properties are the same for both LSMs, for all simulations.

1) ATMOSPHERIC FORCING DATA

We arbitrarily selected a catchment from the Red–Arkansas River basin in the southern Great Plains of the United States to provide many of the model parameter values for the idealized experiment. The catchment is characterized by grass with an average vegetation cover of 70%, loam soil, and moderate topography. For the forcing, we first generated 25 sets of monthly precipitation time series (each series consisting of 200 random monthly totals) with the mean precipitation of each time series varying from 15 to 500 mm. The subsequent temporal disaggregation of the monthly totals was based on the hourly precipitation time series at the chosen catchment for July of 1979 as provided by Project for Intercomparison of Land-surface Parameterization Schemes Phase 2c (PILPS2c; Wood et al. 1998). In essence, for each forcing month, the hourly PILPS2c precipitation data were rescaled by a constant factor to produce the desired monthly total.

Generating a series of radiation forcing data was a bit more complicated. Specifications of downward shortwave and longwave radiation values had to be consistent with specified near-surface air temperature, which in turn had to be consistent with near-surface specific humidity. The procedure we used to generate these data is described in the appendix. The result of the procedure was 20 sets of downward longwave and shortwave radiation, temperature, and humidity data, each set consisting of 200 months of hourly values.

All combinations of the 20 radiation and 25 precipitation time series were used to drive each LSM, yielding a total of 400 different 200-month simulations for each LSM. The actual mean accumulated net radiation for each experiment, once the simulated surface temperature was accounted for, was found to vary from 28 to 412 mm month^{-1} (using latent heat of vaporization to convert energy to water equivalent). Again, the precipitation varied from 15 to 500 mm month^{-1}. The 400 combinations thus sample climates that are cold and wet, cold and dry, hot and dry, hot and wet, and everything in between.

2) EXPERIMENTAL RESULTS

The contour maps in Figs. 1a,b show how the 31-day lagged autocorrelation of soil moisture varies with monthly mean net radiation and precipitation for the two LSMs. Each contour map is based on 400 data values, one for each 200-month simulation. The differences in the autocorrelations produced by the two LSMs is shown in Fig. 1c. Figure 1c indicates that the NSIPP Catchment LSM has larger memory in climates where the monthly mean net radiation is of the same order as monthly mean precipitation. In contrast, the Mosaic LSM seems to have larger memory in climates with low net radiation and high precipitation or with high net radiation and low precipitation—i.e., in cold, wet climates or in hot, dry climates. Note that both LSMs (as applied here) use the same water holding capacity and are forced with essentially the same potential evaporation at any given point on the plot. The fact that their memories still differ illustrates the inadequacy of the practice (e.g., Delworth and Manabe 1988) of relating soil moisture memory to these two quantities alone.

We can employ (4) to explain the differences in memory in terms of differences in model structure. Since this is a perpetual-July experiment, the first term (seasonality; $\sigma_{w_n}/\sigma_{w_{n+1}}$) and the fourth term (persistence in the atmospheric forcing; $\mathrm{cov}(w_n, F_n)/\sigma^2_{w_n}$) of (4) are insignificant. Intermodel differences in the evaporation term ($c\overline{R_n}/C_s$) and the runoff term ($a\overline{P_n}/C_s$) must be behind the differences in Fig. 1c. Furthermore, because C_s, $\overline{R_n}$, and $\overline{P_n}$ are the same in both models at any given point on the contour map, the intermodel differences in the autocorrelation of soil moisture in Fig. 1c must reflect differences in the values of a and c. Recall from section 2 that a describes the sensitivity of runoff ratio to soil moisture and c describes the sensitivity of evaporative fraction to soil moisture.

Figures 1d and 1e show the differences in the $c\overline{R_n}/C_s$ and $a\overline{P_n}/C_s$ terms, respectively (NSIPP Catchment minus Mosaic). Relative to the Mosaic LSM, the NSIPP Catchment LSM has much higher values of $c\overline{R_n}/C_s$ in hot, dry climates, and it has higher values of $a\overline{P_n}/C_s$ in cold, wet climates. Thus, as indicated by (4), soil moisture memory in the NSIPP Catchment LSM is much smaller in these climates. Analysis of the structures of the two LSMs explains, to some extent, these differences in a and c values. In hot, dry climates, soil moisture in the Mosaic LSM's root zone is typically below the wilting point, preventing transpiration. Because the wilting point in the one-dimensional Mosaic LSM is not crossed with a small addition or subtraction of moisture, the sensitivity of total evaporation to variations in profile soil moisture is very small—c in (4) is very small. In the NSIPP Catchment LSM, on the other hand, the relationship between dry conditions and wilting is quite different. As the surface element gets drier, the areal fraction of the root zone undergoing wilting gets larger. Even when a large fraction of the element is experiencing wilting (i.e., even in very hot, dry conditions), the addition or subtraction of additional moisture to the profile can still change the transpiration rate, since it basically acts to change further the areal fraction of wilting. Thus, for the NSIPP Catchment LSM, c can be sizeable even in hot, dry climates.

In cold, wet climates, runoff in both the Mosaic LSM and the NSIPP Catchment LSM is strongly sensitive to soil moisture—a is large for both models. In the Mosaic LSM, drainage out of the soil column increases exponentially with the log of soil moisture to a maximum rate, obtained when the soil is saturated. Similarly, in the NSIPP Catchment LSM, baseflow out of the catchment increases exponentially with soil moisture to the high rate obtained when the soil is saturated (see Fig.

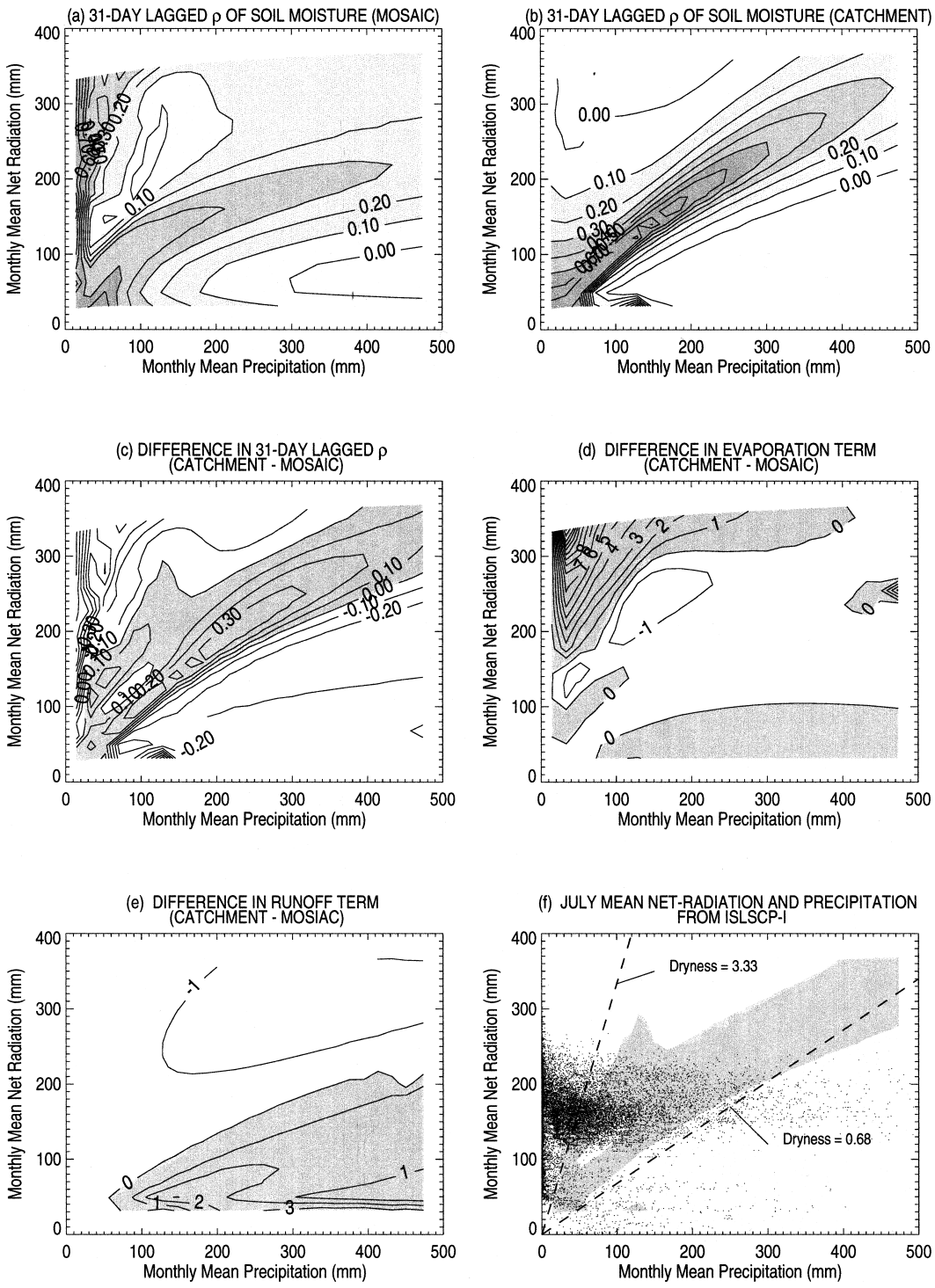

FIG. 1. (a) Contour plot of 31-day-lagged autocorrelation of soil moisture (ρ_{31}) for varying monthly mean precipitation and net radiation for the Mosaic LSM. (b) Corresponding contour plot for the NSIPP Catchment LSM. (c) Differences in ρ_{31} between the two LSMs (NSIPP Catchment minus Mosaic). (d) Differences in evaporation term, $c\overline{R_n}/C_s$ (NSIPP Catchment minus Mosaic). (e) Differences in runoff term, $a\overline{P_n}/C_s$ (NSIPP Catchment minus Mosaic). (f) Points representing pairs of Jul mean net radiation and precipitation values from the global dataset of ISLSCP-I. Approximate lines of constant dryness index ($\overline{R_n}/\overline{P_n}$) bound the shaded region. (c)–(f) Shaded region shows the climates for which NSIPP Catchment's corresponding variable exceeds Mosaic's.

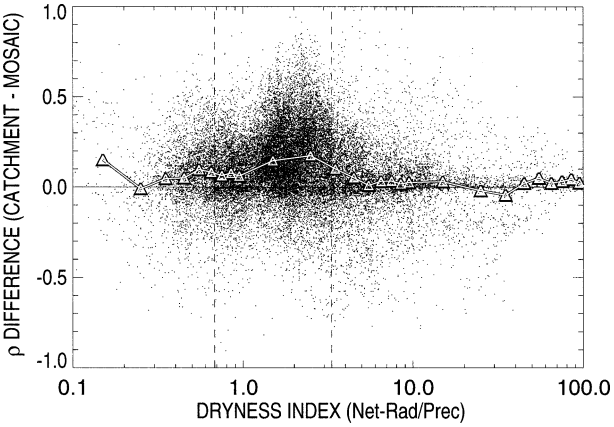

FIG. 2. Plot of differences in 1-month-lagged (JJA) ρ (NSIPP Catchment LSM minus Mosaic LSM) vs dryness index ($\overline{R_n}/\overline{P_n}$). The solid line was obtained through simple binning. The two vertical lines show the climate region ($0.68 < \overline{R_n}/\overline{P_n} < 3.33$) where the Catchment LSM's ρ is greater than that of the Mosaic LSM in the idealized experiment (Fig. 1f). Note that net radiation is scaled by the latent heat of vaporization to make the ratio dimensionless.

2 of Ducharne et al. 2000). The differences seen for cold, wet climates in Fig. 1e simply reflects the fact that the rate of change for wet soils, while high for both models, turns out to be higher for the NSIPP Catchment LSM.

The reason for the NSIPP Catchment LSM's higher memory when precipitation is approximately balanced by net radiation is not as easy to pin down. Consider, though, the argument set forth earlier for hot, dry climates. In these climates, soil moisture reductions lead to reductions in the NSIPP Catchment LSM's evaporation but not the Mosaic LSM's evaporation because in the latter model, evaporation has already been shut off by wilting vegetation. In a sense, this implies that the Mosaic LSM goes from full transpiration to zero evaporation over a smaller soil moisture range. The compressed transition implies that the sensitivity of evaporation to soil moisture over this range (characteristic of intermediate climates) is higher for the Mosaic LSM than for the NSIPP-Catchment LSM, which in turn implies a lower memory for the Mosaic LSM.

To give a rough indication of the relevance of the climates tested in the idealized experiment, we computed the global distributions of July-mean net radiation

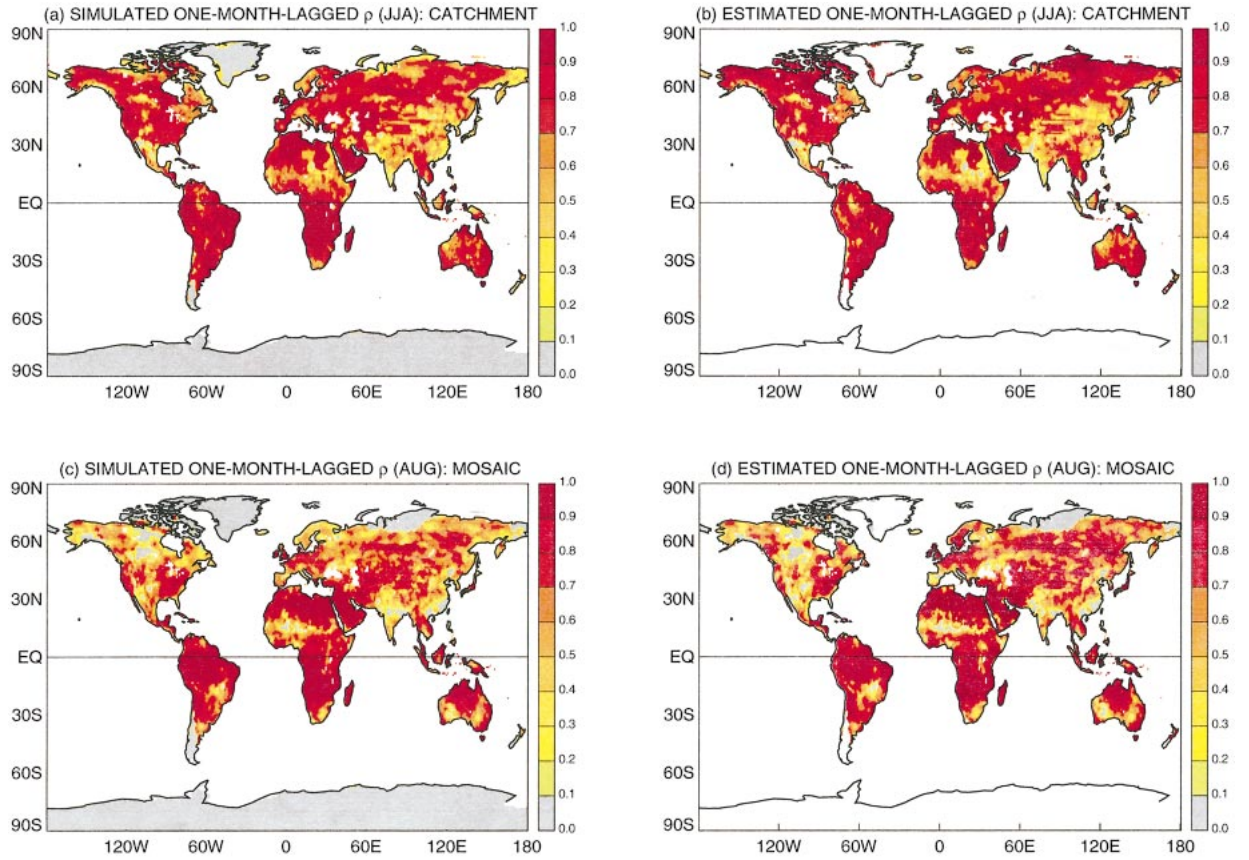

FIG. 3. (a) Global distribution of 1-month-lagged (for JJA) ρ for the NSIPP Catchment LSM. (b) Estimated ρ for JJA using (4) for the NSIPP Catchment LSM. (c) Global distribution of 1-month-lagged ρ (using Aug simulations) for the Mosaic LSM. (d) Estimated ρ for Aug using (4) for the Mosaic LSM.

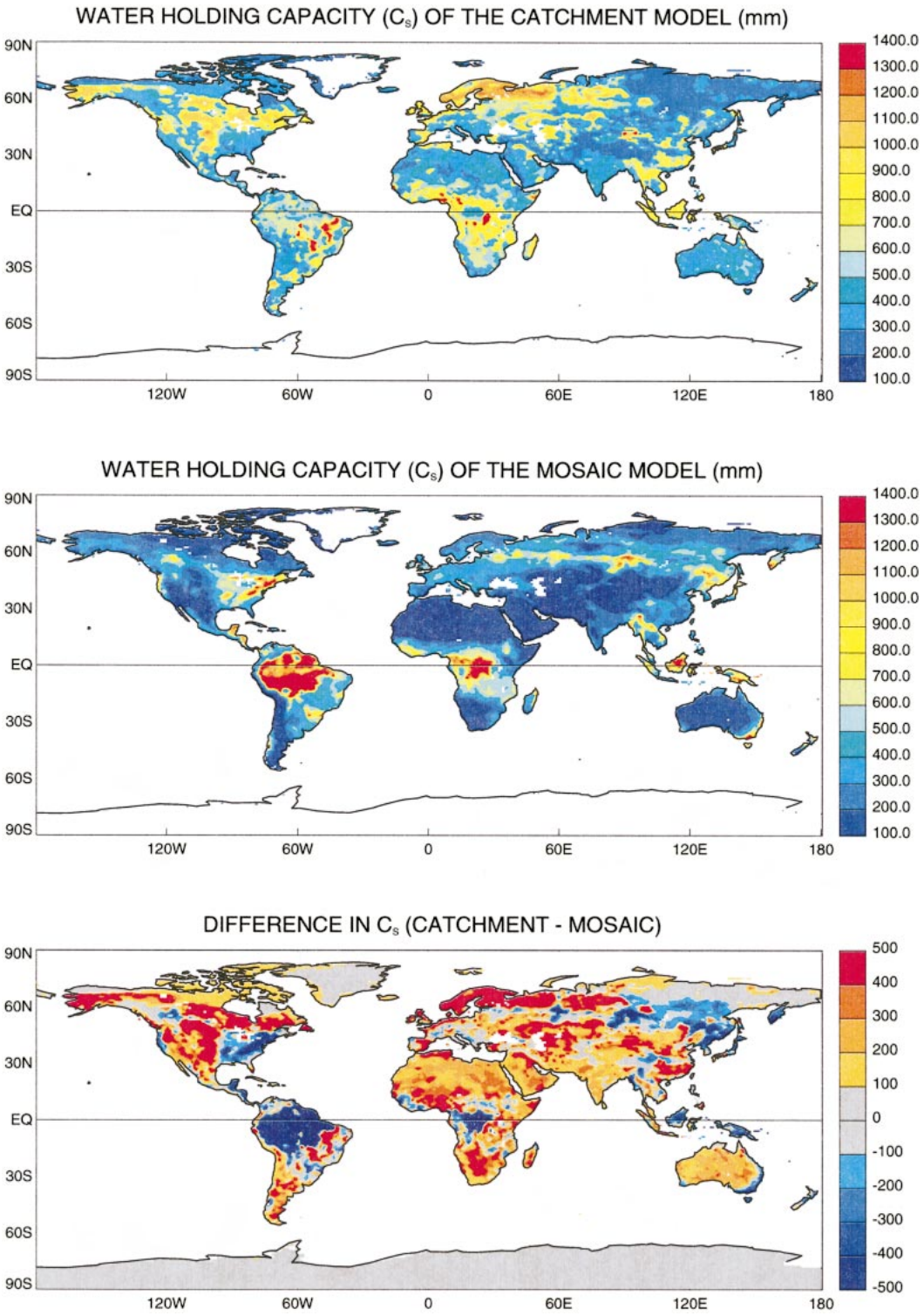

FIG. 4. (top) Map of water holding capacities (mm) (C_s) used by the NSIPP Catchment LSM. (middle) Corresponding map for the Mosaic LSM. (bottom) Differences in C_s (NSIPP Catchment minus Mosaic).

and precipitation from the International Satellite Land Surface Climatology Project Initiative I (ISLSCP-I) dataset (Sellers et al. 1996) on 1° grid cells, using near-surface air temperature to approximate surface temperature for the upwelling longwave radiation calculation. The values over land are plotted on the contour plot of autocorrelation differences (Fig. 1c) to produce Fig. 1f. Note that the climate regime in which the NSIPP Catchment LSM produces a longer memory than the Mosaic LSM is approximately marked in Fig. 1f by lines of constant dryness index ($\overline{R_n}/\overline{P_n}$; dryness index equals 0.68 and 3.3). Figure 1f suggests that for most of the drier areas of the earth, the Mosaic LSM would provide the higher soil moisture memory. The NSIPP Catchment LSM, however, would nevertheless provide the higher memory over a substantial fraction of the land surface, perhaps even the fraction that matters most for seasonal prediction—Koster et al. (2000b) demonstrate the importance of land–atmosphere feedback in regions that are not too dry and not too wet.

Again, it should be noted that this idealized analysis ignores the impacts of seasonality, forcing persistence, and variations in water holding capacity. All aspects of the problem are addressed in our less idealized experiment, discussed next.

b. Global distributions of soil moisture memory

In this section, realistic atmospheric forcing is applied globally to generate soil moisture memory distributions for both LSMs. The earth's land surface was resolved into 36 716 hydrologic catchments through the application of high-resolution (1 km) digital elevation data (Verdin and Verdin 1999). Land cover characteristics, soil hydrologic properties, and topographic characteristics for those catchments were derived from a variety of recent global datasets. Both LSMs used the same distribution of surface elements. That is, the Mosaic LSM was run on the catchment grid, even though it made no use of the topographic information.

1) GLOBAL SOIL MOISTURE MEMORY MAPS

European Centre for Medium-Range Weather Forecasts (ECMWF) 0.5°, 6-hourly global datasets of atmospheric forcing (Berg 2001) processed to allow monthly precipitation and radiation totals to agree with observations, and interpolated onto the catchment grid, were used to force the NSIPP Catchment LSM and the Mosaic LSM over the period 1979–93. We used a two-tile approach to implement the Mosaic LSM onto the catchment grid: one tile in each catchment was assigned to the dominant vegetation, and the other was assigned to bare soil. The fraction of vegetation cover was computed with high-resolution land cover information for each catchment (Guillevic et al. 2002). The NSIPP Catchment LSM assumes one dominant land cover type, though the model has three (four, when snow is present) dynamic tiles corresponding to different soil moisture regimes.

June–July–August (JJA) model diagnostics for the 15 yr were used to compute 1-month-lagged autocorrelation (ρ) of soil moisture in both models. Figure 2 shows a scatterplot of the autocorrelation differences between the two LSMs versus dryness index, $\overline{R_n}/\overline{P_n}$, determined from the forcing alone, that is, by approximating radiative surface temperature with the air temperature. The fitted line, obtained through a simple binning procedure, clearly shows that the NSIPP Catchment LSM tends to have the higher memory when the dryness index is of order 1. This is reminiscent of what was observed in the idealized experiment (Fig. 1c), in which the NSIPP Catchment LSM tended to have higher memory when the monthly mean net radiation $\overline{R_n}$ (in units of water equivalent) and precipitation $\overline{P_n}$ were similar. (For reference, the two dashed lines overlaid on Fig. 2 show the approximate range of dryness index over which the NSIPP Catchment LSM's memory exceeded that of the Mosaic LSM in the idealized experiment.) Figure 2 shows that in hot, dry or cold, wet climates this relative strength disappears. The fact that the Mosaic LSM does not produce a higher memory in the extreme climates is due in part to its lower water holding capacity, as discussed in the next section.

The global simulations allow a further verification (beyond that provided by Koster and Suarez 2001) of the ability of (4) to reproduce ρ. Figure 3a shows the global distribution of ρ (i.e., 1-month-lagged autocorrelation) computed from the boreal summer (JJA) data generated by the NSIPP Catchment LSM. Figure 3b shows the corresponding global distribution of ρ estimated by (4). The agreement between the simulated and estimated ρ values is clearly strong. Similarly, Figs. 3c and 3d show strong agreement between simulated and estimated ρ values for August for the Mosaic LSM. Such agreement strongly supports our use of the Eq. (4) to analyze and contrast the two LSMs.

Note, however, that August values were used instead of JJA values in Figs. 3c,d because of some problems with interpreting the Mosaic LSM data in June and July, for regions north of 45°. Supplemental studies with the Mosaic LSM data show that the tiling approach used by Mosaic—particularly our use of catchment-averaged quantities rather than tile quantities in the memory analysis—compromises the effectiveness of (4) in high latitudes during these months, possibly because of the impact of recently melted snow water. Indeed, a one-tile-per-catchment repeat of the Mosaic LSM experiment produced an excellent agreement between simulated and estimated ρ in June and July across the globe. In any case, this limitation in high latitudes for the tile-average quantities should be kept in mind when interpreting the results below.

2) WATER HOLDING CAPACITY

Some prior works (e.g., Delworth and Manabe 1988) suggest that the key LSM parameter affecting soil mois-

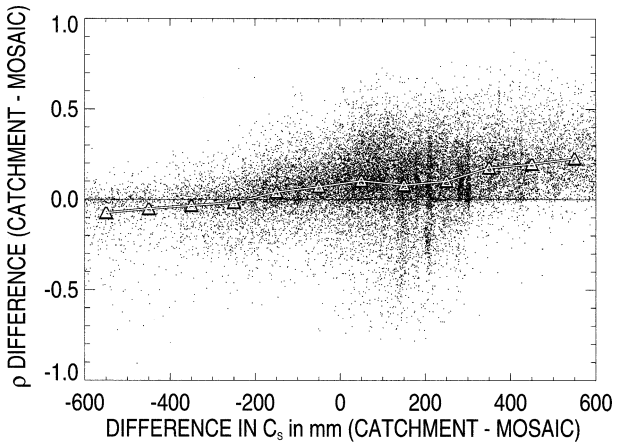

FIG. 5. Plot of differences in 1-month-lagged ρ (JJA) vs difference in C_s. The solid line was obtained through simple binning.

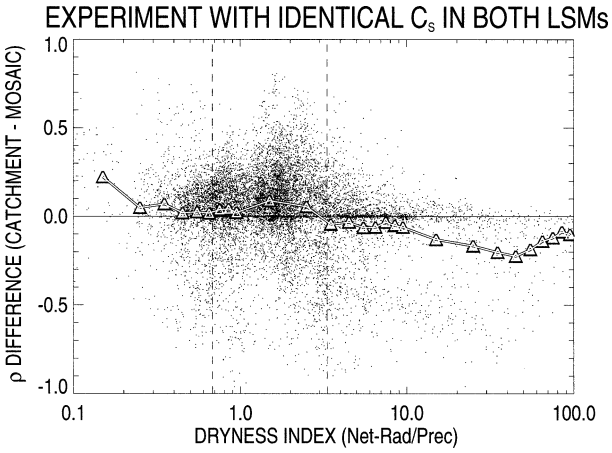

FIG. 6. The same as in Fig. 2 except experiment with identical C_s in both LSMs. Plot of differences in 1-month-lagged (JJA) ρ (NSIPP Catchment LSM minus Mosaic LSM) vs dryness index ($\overline{R_n}/\overline{P_n}$). The solid line was obtained through simple binning. The two vertical lines show the climate region ($0.68 < \overline{R_n}/\overline{P_n} < 3.33$) where the Catchment LSM's ρ is greater than that of the Mosaic LSM in the idealized experiment (Fig. 1f). Note that net radiation is scaled by the latent heat of vaporization to make the ratio dimensionless.

ture memory is water holding capacity. Two of the terms in (4) indeed include C_s directly, and C_s also appears in the definition of F_n. A separate consideration of C_s is thus warranted.

Figures 4a,b show the global distribution of column water holding capacity (C_s) for the two LSMs. Since the Mosaic LSM as employed here uses two separate tiles within each computational catchment (one for vegetation and one for bare soil), and since these tiles can be hydrologically active at different levels, an effective C_s value was computed for each catchment following the procedure described in Koster and Suarez (2001). The difference in C_s between the NSIPP Catchment LSM and the Mosaic LSM is shown in Fig. 4c. The NSIPP Catchment LSM has the higher C_s over most of the globe, though that in the Mosaic LSM is higher in the Amazon and Congo River basins, in the eastern United States, and in northeast Asia. Note that the two LSMs define C_s in distinctly different ways. The NSIPP Catchment LSM defines water holding capacity as the capacity above the wilting point within the soil profile down to the bedrock. The ISLSCP-I (Sellers et al. 1996) global distribution of soil profile depth dataset is used to estimate the depth to bedrock in each catchment. In the Mosaic LSM, on the other hand, the computed effective water holding capacity is a function of the vegetation type and is not keyed to any dataset of soil profile depth. Differences in C_s between the two LSMs are therefore not surprising.

A scatterplot of the autocorrelation differences versus differences in water holding capacity is shown in Fig. 5. A tendency for an increase in the intermodel ρ difference with an increase in the intermodel C_s difference is indicated by the fitted line, obtained through a simple binning procedure. The tremendous scatter around the line, however, indicates that differences in water holding capacity explain only part of the distinction in the LSMs' memory behaviors. The LSMs' runoff and evaporation parameterization schemes (through a and c) must also exert control over the soil moisture memory.

3) REMOVING THE IMPACT OF WATER HOLDING CAPACITY

In order to remove the impact of water holding capacity differences on the simulated memory, we carried out an additional 15-yr global simulation using the computed effective C_s for the Mosaic LSM in the NSIPP Catchment LSM. Figure 6 shows how the scatterplot in Fig. 2 (autocorrelation differences between the two LSMs vs dryness index, $\overline{R_n}/\overline{P_n}$) looks when both LSMs use the same C_s values. The figure shows a reduction of memory for the NSIPP Catchment LSM in hot, dry climates when Mosaic's C_s is used (cf. Fig. 2).

We employed (4) to characterize the intermodel ρ differences. Since the same atmospheric forcing was used in both LSMs, differences in two of the controls in (4)—seasonality ($\sigma_{w_n}/\sigma_{w_{n+1}}$) and persistence [$\mathrm{cov}(w_n, F_n)/\sigma^2_{w_n}$]—will have limited effect on the intermodel ρ differences. The ρ differences will thus reflect the differences in the other two terms; the variation of evaporation with soil moisture ($c\overline{R_n}/C_s$) and the variation of runoff with soil moisture ($a\overline{P_n}/C_s$). Furthermore, assuming differences in mean net radiation ($\overline{R_n}$) between the two LSMs are negligible, and given the use of the same C_s values in both LSMs, the ρ differences essentially reflect differences in the values of a and c. Equation (4) implies that higher values of a and c lead to reduced values of soil moisture memory. The values of a and c for each model were computed using JJA diagnostics.

A map of the differences in ρ between the two LSMs (when run with identical water holding capacities) is

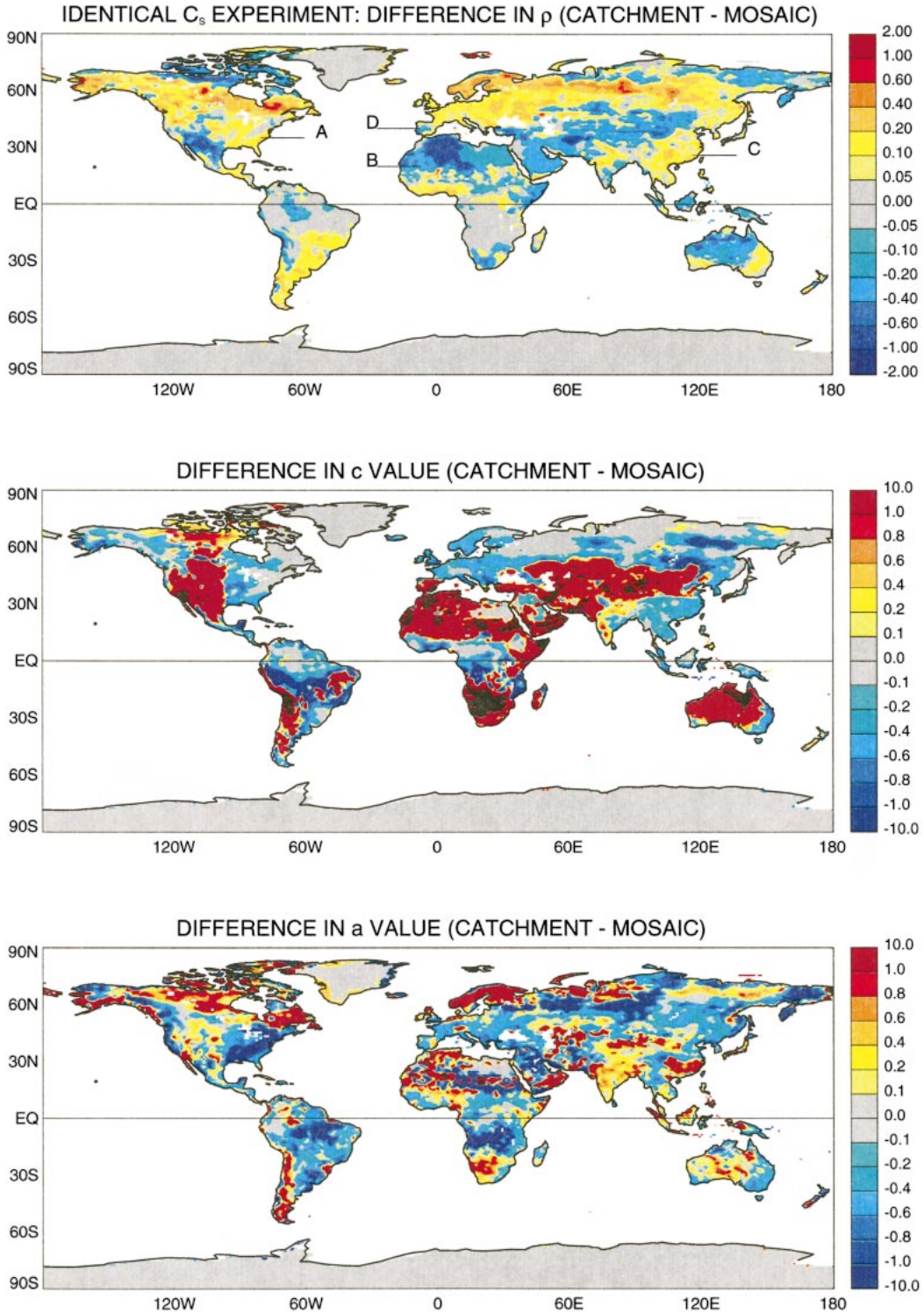

FIG. 7. Experiment in which both LSMs use the same water holding capacities. (top) Map of differences in 1-month-lagged ρ (JJA) (NSIPP Catchment minus Mosaic). (middle) Differences in c [Eq. (3)]. (bottom) Differences in a [Eq. (2)].

shown in Fig. 7a. Figures 7b,c show the global distributions of the intermodel differences in *c* and *a*. The four areas indicated in Fig. 7a serve to illustrate the intermodel differences uncovered in this analysis.

In area A, in the eastern United States, the NSIPP Catchment LSM shows a longer memory than the Mosaic LSM. This is because in area A, NSIPP Catchment's evaporation and runoff are less sensitive to soil moisture variations (cf. Mosaic), as indicated by the smaller values of *a* and *c* in Figs. 7b,c. In area B (North Africa), the lower memory of the NSIPP Catchment LSM is due to its higher evaporation and runoff sensitivities there. Area C, in southeast China, shows a higher memory for the NSIPP Catchment LSM; the lower *c* value counteracts the effect of the higher *a* value there. (It is important to remember here that the magnitudes of *a* and *c* cannot be directly compared with each other; the relevant quantities to compare are $c\overline{R_n}$ and $a\overline{P_n}$.) Finally, in area D (Spain), the higher *c* value of the NSIPP Catchment LSM overwhelms the effect of the lower *a* value there, leading to a lower soil moisture memory.

5. Discussion and summary

In this paper, we address the problem of characterizing intermodel differences in simulated soil moisture memory. We use as a framework for this analysis the autocorrelation equation, (4), derived by Koster and Suarez (2001). The equation helps explain differences in memory in terms of differences in the structures of the LSMs. The relevance of the equation to this analysis is confirmed by the agreement in Fig. 3 between the autocorrelations estimated by the equation and those actually simulated by the two LSMs studied.

The idealized experiment in section 4a contrasted the LSM behaviors in a multitude of different climates, isolating in particular the way in which their evaporation and runoff production mechanisms affect simulated memory. While the experiment was limited by the neglect of land cover, soil, and water holding capacity differences between the LSMs (a deficiency that could, in principle, be overcome by repeating the experiment many times, under many different sets of surface properties), it does indicate that the NSIPP catchment LSM tends to have higher soil moisture memory when precipitation and net radiation (scaled into units of water equivalent) are approximately in balance. A similar conclusion is reached through analysis of the less idealized, global memory calculations in section 4b(1) (see Fig. 2). The reasons for the difference in model behavior involve intermodel differences in the sensitivities of runoff and evaporation to soil moisture, as embodied in the parameters *a* and *c* of (4). When precipitation and net radiation are roughly equal, the sensitivities are, for various reasons, smaller in the NSIPP Catchment LSM (Figs. 1d,e), and thus memory in this model is higher. When precipitation overwhelms net radiation, the NSIPP Catchment LSM's baseflow rate becomes more responsive to changes in soil moisture than the Mosaic LSM's drainage rate, leading to a higher *a* value and thus to lower memory relative to the Mosaic LSM. When net radiation overwhelms precipitation, the ''dynamic wilting area'' in the NSIPP Catchment LSM—absent in the Mosaic LSM—gives it a higher evaporation sensitivity to soil moisture (a higher *c* value) and thus a lower soil moisture memory.

As an aside, we note that for seasonal prediction, the sensitivity of evaporation to soil moisture should be neither too high nor too low. When the sensitivity is too high, soil moisture memory is reduced, as discussed earlier. When it is too low, however, the atmosphere cannot respond to a soil moisture anomaly, even if it persists well into the forecast period (Koster and Suarez 2003). These two opposing effects suggest the existence of an optimal, intermediate value for the sensitivity. This is being explored in ongoing research.

The influence of intermodel differences in water holding capacity (C_s) on memory was given some attention, given the importance that many past works on memory have assigned to this parameter (e.g., Vinnikov and Yeserkepova 1991; Entin et al. 2000). Figure 5 shows that intermodel differences in simulated memory do tend to grow with intermodel differences in water holding capacity. The huge noise in the plot, however, indicates that C_s is not the only parameter, and perhaps not even the most important parameter, controlling memory. As noted previously, and as illustrated in section 4b(3), intermodel differences in evaporation and runoff sensitivities to soil moisture also play a critical role.

An obvious question arises from this work, namely, which of the two LSMs simulates the most realistic soil moisture memory? Although a definitive answer to this question cannot be given now due to a paucity of decadal data on the global scale, the analysis described earlier does point to what may be a viable approach for evaluating global simulated memory in the near term. First, note that a direct evaluation of simulated memory against in situ soil moisture observations at the global scale is hampered by the requirement of decades of areally averaged observations, for such measurements essentially do not exist (outside of point measurements in Asia and Illinois), even for the present day. Global fields of soil moisture from remotely sensed data may overcome this deficiency, though the buildup of the necessary data would, again, take decades. Simulated soil moisture memory, however, can perhaps be validated much sooner by validating the simulation of the physical controls over this memory, as embodied in (4). A few years' worth of soil moisture, evaporation, runoff, precipitation, and net radiation data, if an appropriate measurement network could be developed, might be adequate to quantify the terms in (4) that the LSMs need to match.

Given the implications of soil moisture memory to seasonal prediction and other scientific problems, there is an acute need to contrast and evaluate the memory

simulated by the various LSMs coupled to atmospheric GCMs. The framework utilized in this paper provides a means to perform such an analysis. Of course, when considering coupled land–atmosphere models, analysis of errors in simulated precipitation and net radiation is probably just as important as analyzing the a, c, and C_s values that underlie the LSM.

Acknowledgments. We thank Chris Milly, Guido Salvucci, and an anonymous reviewer for for insightful reviews. This research work was supported by funding from the Earth Science Enterprise of NASA Headquarters through the EOS-Interdisciplinary Science Program and the NASA Seasonal-to-Interannual Prediction Project (NSIPP). The NASA Center for Computational Sciences provided computational resources for the global offline simulations. J. Famiglietti, A. Berg, and S. Holl of the University of California, Irvine, provided the 0.5° global gridded atmospheric forcings for 1979–93, and Colin Stark of Lamont-Doherty Earth Observatory processed catchment characteristics provided by the USGS EROS Data Center.

APPENDIX

Generation of Radiation Forcing Data for the Idealized Experiment

An approximate emissivity ϵ of the overlying atmosphere was found by regressing downward longwave radiation (R_{LW}) against σT_a^4, where T_a is the surface air temperature and σ is the Stefan–Boltzmann constant, in a way that forces the fitted line through the origin:

$$R_{\mathrm{LW}} = \epsilon\sigma T_a^4. \tag{A1}$$

The values of R_{LW} and T_a were taken from hourly PILPS2c data for July for 10 yr over the Red–Arkansas River basin.

Global ISLSCP-I data (Sellers et al. 1996) for July 1987 provided 600 1° grid cells that represented well the global variability of July 1987 radiation forcing. A linear relationship between the monthly mean surface air temperature ($\overline{T}_a$) and monthly accumulated net radiation ($\overline{R}_{\mathrm{net}}$) was derived using linear regression analysis between $\overline{T}_a$ and $\overline{R}_{\mathrm{net}}$ of the chosen grid cells. Here, $\overline{R}_{\mathrm{net}}$ was computed through a radiation budget computation on each grid cell, assuming that the radiative surface air temperature approximately equals T_a for the upward longwave radiation calculation. The linear regression analysis yielded an equation:

$$\overline{T}_a = 0.15868\ \overline{R}_{\mathrm{net}} + 268.607. \tag{A2}$$

To generate a set of 20 different radiation time series for the idealized experiment, we first produced the hourly time series $R_{\mathrm{net}}^{79\mathrm{Jul}}$ for the chosen Red–Arkansas catchment. We then multiplied this time series by 20 different values of λ, varying from 0.1 to 2 in increments of 0.1. A λ of 1.0 thus represents no adjustment to the original time series. The corresponding monthly mean temperature ($\overline{T}_{\mathrm{new}}$) for the adjusted monthly net radiation was approximated using (A2).

If the mean air temperature of the PILPS2c forcing for the chosen catchment for July 1979 is $\overline{T}_{79\mathrm{Jul}}$, the downward longwave radiation bias ($R_{\mathrm{LW-bias}}$) we apply is computed as

$$R_{\mathrm{LW-bias}} = \epsilon\sigma(\overline{T}_{\mathrm{new}}^4 - \overline{T}_{79\mathrm{Jul}}^4), \tag{A3}$$

with ϵ taken from (A1). The surface air temperature bias is $\overline{T}_{\mathrm{new}} - \overline{T}_{79\mathrm{Jul}}$. For the net shortwave radiation, let $\overline{R}_{\mathrm{netSW}}^{79\mathrm{Jul}}$ represent the monthly total from the PILPS2c dataset. Through energy balance considerations, we compute an adjustment factor, $\lambda_{R\mathrm{sw}}$, used to scale hourly PILPS2c downward shortwave radiation for the month of July 1979 as

$$\lambda_{R\mathrm{sw}} = 1 + \left[(\lambda - 1)\overline{R}_{\mathrm{net}}^{79\ \mathrm{Jul}} - \left(1 - \frac{1}{\epsilon}\right)R_{\mathrm{LW\text{-}bias}}\right]\frac{1}{\overline{R}_{\mathrm{netSW}}^{79\ \mathrm{Jul}}}, \tag{A4}$$

where ϵ is computed with (A1) and ($R_{\mathrm{LW-bias}}$) is computed with (A3). The hourly PILPS2c forcing for the month of July 1979 for the chosen catchment was adjusted using the above biases to obtain 20 sets of downward shortwave and longwave radiation and surface air temperature time series, one for each of the 20 values of λ (λ = 0.1, 0.2, 0.3, . . . , 2.0). For each dataset, specific humidity of the air was adjusted to maintain the same relative humidity as observed. The month-long datasets so-derived were each repeated 200 times in order to be used in conjunction with the 200-month precipitation datasets.

REFERENCES

Berg, A. A., 2001: The sensitivity of land surface model simulations to bias correction of the European Center for Medium-Range Weather Forecasts reanalysis. M.S. thesis, Dept. of Geological Sciences, University of Texas at Austin, 115 pp.

Delworth, T. L., and S. Manabe, 1988: The influence of potential evaporation on the variabilities of simulated soil wetness and climate. *J. Climate,* **1,** 523–547.

Dirmeyer, P. A., 2000: Using a global soil witness dataset to improve seasonal climate simulation. *J. Climate,* **13,** 2900–2922.

Ducharne, A., R. D. Koster, M. J. Suarez, M. Stieglitz, and P. Kumar, 2000: A catchment-based approach to modeling land surface processes in a general circulation model. Part 2: Parameter estimation and model demonstration. *J. Geophys. Res.,* **105** (D20), 24 823–24 838.

Entin, J. K., A. Robock, K. Y. Vinnikov, S. E. Hollinger, S. Liu, and A. Namkhai, 2000: Temporal and spatial scales of observed soil moisture variations in the extratropics. *J. Geophys. Res.,* **105** (D9), 11 865–11 877.

Guillevic, P., R. D. Koster, M. J. Suarez, L. Bounoua, G. J. Collatz, S. O. Los, and S. P. P. Mahanama, 2002: Influence of the interannual variability of vegetation on the surface energy balance—A global sensitivity study. *J. Hydrometeor.,* **3,** 617–629.

Koster, R. D., and M. J. Suarez, 1992: Modeling the land surface boundary in climate models as a composite of independent vegetation stands. *J. Geophys. Res.,* **97,** 2697–2716.

——, and ——, 1995: The relative contributions of land and ocean process to precipitation variability. *J. Geophys. Res.,* **100,** 13 775–13 790.
——, and ——, 1996a: Energy and water balance calculations in the MOSAIC LSM. NASA Tech. Memo. 104606, Vol. 9, 60 pp.
——, and ——, 1996b: The influence of land surface moisture retention on precipitation statistics. *J. Climate,* **9,** 2551–2567.
——, and P. C. D. Milly, 1997: The interplay between transpiration and runoff formulations in land surface schemes used with atmospheric models. *J. Climate,* **10,** 1578–1591.
——, and M. J. Suarez, 2001: Soil moisture memory in climate models. *J. Hydrometeor.,* **2,** 558–570.
——, and ——, 2003: Impact of land surface initialization on seasonal precipitation and temperature prediction. *J. Hydrometeor.,* **4,** 408–423.
——, ——, A. Ducharne, M. Stieglitz, and P. Kumar, 2000a: A catchment-based approach to modeling land surface processes in a general circulation model. Part 1: Model structure. *J. Geophys. Res.,* **105** (D20), 24 809–24 822.
——, ——, and M. Heiser, 2000b: Variance and predictability of precipitation at seasonal-to-interannual timescales. *J. Hydrometeor.,* **1,** 26–46.
Liu, Y., and R. Avissar, 1999a: A study of persistence in the land–atmosphere system using a fourth-order analytical model. *J. Climate,* **12,** 2154–2168.
——, and ——, 1999b: A study of persistence in the land–atmosphere system using a general circulation model and observations. *J. Climate,* **12,** 2139–2153.
Oglesby, R. J., and D. J. Erickson III, 1989: Soil moisture and the persistence of North American drought. *J. Climate,* **2,** 1362–1380.
Robock, A., K. Y. Vinnikov, G. Sirinivasan, J. K. Entin, S. E. Hollinger, N. A. Speranskaya, S. Liu, and A. Namkhai, 2000: The global soil moisture data bank. *Bull. Amer. Meteor. Soc.,* **81,** 1281–1299.
Sellers, P. J., Y. Mintz, Y. C. Sud, and A. Dalcher, 1986: A simple biosphere model (SiB) for use within general circulation models. *J. Atmos. Sci.,* **43,** 505–531.
——, and Coauthors, 1996: The ISLSCP Initiative I global datasets: Surface boundary conditions and atmospheric forcings for land–atmosphere studies. *Bull. Amer. Meteor. Soc.,* **77,** 1987–2005.
Shukla, J., and Y. Mintz, 1982: Influence of land-surface evapotranspiration on the earth's climate. *Science,* **215,** 1498–1501.
Verdin, K. L., and J. P. Verdin, 1999: A topological system for delineation and codification of the Earth's river basins. *J. Hydrol.,* **218,** 1–12.
Vinnikov, K. Ya, and I. B. Yeserkepova, 1991: Soil moisture: Empirical data and model results, *J. Climate,* **4,** 66–79.
——, A. Robock, N. A. Speranskaya, and A. Schlosser, 1996: Scales of temporal and spatial variability of midlatitude soil moisture. *J. Geophys. Res.,* **101** (D3), 7163–7174.
Wood, E. F., and Coauthors, 1998: The Project for Intercomparison of Land-Surface Parameterization Schemes (PILPS) Phase 2(c) Red-Arkansas River Basin experiment: 1. Experiment description and summary intercomparisons. *Global Planet. Change,* **19,** 115–135.